High speed and safe mobile robot control in unstructured environments

Roland Lenain, Mathieu Richier, Jean-Baptiste Braconnier, Christophe Cariou, Benoit Thuilot

***Abstract*—Interventions in emergency situations require to be fast, accurate and safe, in order to bring a quick assistance. As it may often be risky for people to bring a direct assistance, the use of automatic devices, such as mobile robots, in a first step can offers a safe solution. Nevertheless, it implies the motion control on low structured environment moreover at important speed. This may generate important perturbations with respect to classical motion control law, which cannot be considered in such applications. In this paper, a new control approach, taking into account natural ground characteristics is proposed, in order to preserve the accuracy and stability of the robot. An adaptive and predictive control algorithm is firstly designed, based on both an extended kinematic and a dynamic representation. It permits to address path tracking in harsh conditions and preserve a high level of accuracy without considering the robot stability in a first step. In addition, an active velocity and trajectory management algorithm is developped from control point of view to avoid the rollover risk and obstacle collision thanks to the notion of traversability. Since the adaptive control law estimates the dynamic parameters of the robot (grip conditions, centre of gravity position), a 3D model is available and a stability metric is evaluated in real time. Beyond this evaluation, a predictive control principle is deduced to compute the maximal admissible control variables to preserve the robot stability (i.e. robot maximal velmocity). Such maximal robot action is then merge to a 3D digital map obtained via Lidar sensor, in order to evaluate stability along its expected trajectories, and select the best way with the highest reachable speed. Capabilities of such approach is investigated through full scale experiments.**

***Index Terms*—Path tracking control, off-road mobile robots, stability control, rollover prevention, adaptive and predictive control**

I. Introduction

Off-road mobile robots appear as an interesting solution to answer future needs in various fields of application [29], such as farming [9], surveillance [27], or military activities. However, if many potential devices can benefit from innovation in this area (increased work accuracy, decreased level of risk), such applications require highly accurate control laws, able to preserve accuracy and stability even at high speed. Numerous approaches have been proposed for both motion control and vehicle stability in urban or on-road contexts. Based on kinematic [17] or dynamic [7] models, several control techniques have indeed been developed to achieve accurate path tracking (see for instance [2], [16] or [30]). Beyond motion servoing, the proposed work can be used to improve vehicle stability, even when manually driven. Several solutions have then proposed in the robotics community: steering and braking control ([28] and [1]) or Electronic Stability Program (ESP) systems [3] are two examples of stability devices. However, since car-like vehicles are supposed to move on high-grip ground, such devices and control laws generally assume rolling without a sliding component, or only pseudo-sliding with constant tire cornering stiffnesses. As a result, their direct application in off-road conditions leads to unsatisfactory results.

Indeed, in an off-road mobile robot context, the complexity and the variability of the phenomena encountered have to be tackled to ensure both accuracy and safety. From a simple control point of view, some studies have addressed this point, mainly by considering sliding as a perturbation of a nominal model (kinematic or assuming constant grip conditions). Such a perturbation is then rejected using robust control approaches, such as those proposed in [6] or [14], while [15] acts differentially on each wheel speed to reduce the influence of sliding on the global robot dynamics. Nevertheless, such approaches appear to be conservative, and since grip conditions are not explicitly known, they cannot be re-used for stability purposes, which also depend on such conditions (as can be noticed when considering stability metrics).

This paper proposes a path-tracking algorithm dedicated to mobile robots moving at high speed in off-road conditions, whilst ensuring their stability. As pointed out in [23], rollover may occur quite easily in the rough terrains under consideration. Typically, path tracking control laws do not account for such a risk, and the motion imposed to follow the desired trajectory may lead to hazardous situations (when following a curve at high speed, for instance). In the proposed solution, the perturbations linked to the variable grip conditions mentioned above are tackled thanks to a multi-model observer, based on [13], mixing kinematic and dynamic modeling. It enables a real-time estimation of the ground contact properties, which are consequently taken into account through an adaptive and predictive control scheme acting at two levels: one controlling the steering angle (for path tracking) and the second controlling the robot's linear velocity (for robot stability). This control strategy is as follows: first a nonlinear control law, accounting for sliding thanks to a model-based adaptive approach, is designed. Predictive curvature servoing is added in order to anticipate actuator settling time and robot inertia. Such a control system is designed to obtain lateral behavior independent from robot velocity. Provided that the desired path is dynamicly achievable, the robot's speed can then be modified without impacting tracking performances. Usually fixed to a constant set point, this variable is here modulated

Alla authors except B. Thuilot are members of Irstea, TSCF Unit Clermont-Ferrand, France. e-mail: firstname.lastname@irstea.fr

B. Thuilot is member of the Lasmea CNRS laboratory, Clermont-Ferrand, France.

in order to ensure robot stability thanks to the prediction of rollover risk.

Such a prediction is made possible thanks to the real-time evaluation of a stability metric. In this paper the Lateral Load Transfer (LLT - [10]), already elaborated in previous work [5], is considered. Its advantages, with respect to other stability metrics such as the Static Stability Factor (SSF) [19], the force-angle measurement criterion [21] - [8] or the Zero Moment Point (ZMP - usually proposed to investigate humanoid and mobile robot stability, [26]) are that on the one hand it does not demand a huge and expensive perception system, and on the other hand it is not dependent on thresholds which are particularly difficult to tune in an outdoor environment. Moreover, the computation of such a metric relies particularly on grip conditions (adapted with the observer designed for path tracking purposes) and on robot velocity, which is considered as a free parameter in steering control. As a result, this last variable can be modulated to regulate the selected metric. A control law relying on the Predictive Functional Control principle (PFC - [25]) is then designed to calculate, in real time, the velocity leading to a critical value of the stability metric in the near future. Such a value can be considered as the maximum admissible velocity for the robot to ensure stable behavior. As a result, the lower of the two values for the desired and the maximum admissible velocity is imposed on the robot, so that the mobile robot can accurately follow a desired trajectory as fast as possible from a stability point of view, whatever the grip conditions.

The paper is organized as follows. First, different levels of modeling, representative of the robot dynamics and accounting for low and variable grip conditions, are presented. These models enable a multi-scale observer, detailed in the second part, to be designed. It supplies a real-time estimation of the variables and parameters representative of off-road dynamics: sideslip angles and tire cornering stiffnesses. Once these variables are provided by the observer, the models used for control design are entirely known. The control strategy is then derived in two steps: path tracking and velocity control. The capabilities of the proposed control strategy are investigated in actual experiments on an off-road mobile robot, able to reach a speed of $7m.s^{-1}$. These show the efficiency of the approach for accurate and safe path tracking in off-road conditions.

II. Mobile robot modeling

Usually, vehicle dynamics are derived from a representation based on the assumption of rolling without sliding at the tire/ground contact point (see for instance [17]). If such a hypothesis is relevant in the urban vehicle context, its direct transposition to all-terrain vehicle leads to inaccurate results. In order to be representative of vehicle motion in an off-road context, low grip conditions have to be properly modeled. Although complete models can be derived from mechanical equations (such as Newton-Euler principles), they appear to be insufficiently flexible for control purposes. Numerous parameters are indeed required, but they appear to be hard to measure and potentially variable in a natural environment. In this paper, an alternative representation is proposed for both motion and stability control. It is based on a multi-model approach, taking advantage of both kinematic and dynamic levels, without requiring the knowledge of numerous parameters. As depicted in Fig. 1, three modeling levels are then considered for different purposes:

- First, an "extended kinematic model" is derived. It consists of adding sideslip angles to a pure kinematic approach to preserve its relevancy with respect to sliding effects. The preservation of a kinematic structure enables a suitable control law to be derived easily, ensuring accurate motion control as soon as the sideslip angles are correctly estimated.
- The second representation is a partial dynamic yaw model, allowing dynamic effects to be accounted for to preserve the reactivity of the global algorithm. This model is considered for the estimation of cornering stiffnesses. Their estimation permits to reconstruct in real time the sideslip angles used in the "extended kinematic model" so as to compute the motion control law.
- Finally, a partial dynamic roll model is computed in order to describe rollover behavior. It takes into account the cornering stiffnesses (estimated thanks to the previous representation levels) and suspension properties in order to compute the Lateral Load Transfer variation and to preserve the robot's dynamic stability.

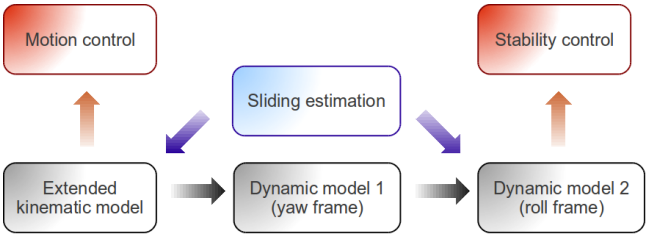

Fig. 1. Interaction scheme of considered models

A. Vehicle kinematic model

As is typaically the case in mobile robot control, the motion is here described thanks to a bicycle representation, where two wheels are considered (one for the front axle and the other for the rear axle). Contrary to [17], in which the directions of the speed vectors are directly superposed with the tire orientation, two sideslip angles are considered here. These variables, α_f and α_r (respectively for the front and rear axle), allow for sliding effects to be accounted for in the robot's motion. Moreover, as path tracking control in off-road conditions is addressed here, vehicle modeling is derived with respect to the path to be followed (denoted Γ). The notations used in the following (see also Fig. 2) are:

- $R_0(x_0, y_0, z_0)$ is the frame attached to the ground,
- A and B are respectively the centers of the front and rear axles, where the virtual wheels of the bicycle model are located. B is the point to be controlled.
- v is the vehicle linear velocity at point B, assumed to be strictly positive, and v_F denotes the linear velocity at the center A of the front wheel.

- δ is the front steering angle. It constitutes the second control variable.
- α_f and α_r are the front and rear tire sideslip angles.
- M is the point on the reference path Γ, which is closest to B. M is assumed to be unique.
- s is the curvilinear abscissa of point M along Γ.
- $I(s)$ denotes the curvature center of path Γ at point M, so that $c(s)$ is the curvature of Γ at that point.
- y is the vehicle lateral deviation at point B with respect to Γ.
- ψ is the orientation of the vehicle centerline with respect to an absolute frame $R_0(x_0,y_0,z_0)$.
- $\psi_\Gamma(s)$ is the orientation of the tangent to Γ at point M with respect to $R_0(x_0,y_0,z_0)$.
- $\tilde{\psi} = \psi - \psi_\Gamma(s)$ is the vehicle angular deviation with respect to Γ.
- L is the vehicle wheelbase.

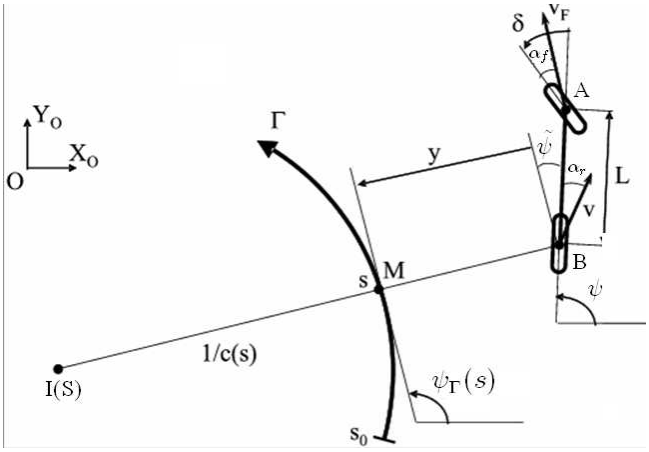

Fig. 2. Path tracking parameters

It can be established (see [17] for model derivation in the non-sliding case and [11] for the integration of sideslip angles) that:

$$\begin{cases} \dot{s} &= v\ \frac{\cos(\tilde{\psi}+\alpha_r)}{1-c(s)y} \\ \dot{y} &= v\ \sin(\tilde{\psi}+\alpha_r) \\ \dot{\tilde{\psi}} &= v\left[\cos(\alpha_r)\lambda_1 - \lambda_2\right] \end{cases} \tag{1}$$

$$\text{with: } \lambda_1 = \frac{\tan(\delta+\alpha_f)-\tan(\alpha_r)}{L},\ \lambda_2 = \frac{c(s)\cos(\tilde{\psi}+\alpha_r)}{1-c(s)y}$$

It can be observed that this model becomes singular when $y = \frac{1}{c(s)}$, i.e. when B is superposed with $I(s)$. This problem is not encountered in practice, since on the one hand actual path curvatures are quite small, and on the other hand the vehicle remains close to Γ when properly initialized. The lateral deviation is thus always smaller than the radius of curvature of Γ.

As described in [13], as soon as α_f and α_r are correctly known, such a model allows robot motion to be accurately decribed, when still preserving a kinematic structure. This is interesting from a control point of view, since this kind of model can be turned into an exact linear form, making it easier to computate a control law (as detailed in Section IV-A)

B. Vehicle dynamic model

Since model (1) is based on a kinematic representation, it does not account for dynamic effects (such as inertia). As a result, the possible estimation of sideslip angles relying on this model (as in [11]) is not reactive enough at high speed. To go further and improve observer reactivity, a dynamic framework is required. Moreover, the description of rollover motion relies mainly on dynamic effects and two representations are then introduced: one is a yaw representation (Fig. 3(a)) and the other is a roll representation (Fig. 3(b)). The yaw model aims at describing the overall vehicle motion on the ground and consists of a bicycle model of the mobile robot. It is used to estimate some vehicle motion variables (such as the lateral acceleration of the vehicle center of gravity) and sideslip angles. As already depicted in Fig. 1, these variables are then injected into the second part of the dynamic model, characterized by a roll 2D projection (shown on Fig. 3(b)), used to compute roll angle, roll rate and finally the *LLT*. The notations used in this paper, and used in Fig. 3(a) and Fig. 3(b), are listed below:

- $R_1(x_1,y_1,z_1)$ is the yaw frame attached to the vehicle,
- $R_2(x_2,y_2,z_2)$ is the roll frame attached to the suspended mass,
- φ_v is the roll angle of the suspended mass,
- β is the global sideslip angle, i.e. the sideslip angle at the vehicle center of gravity,
- u is the linear velocity at the roll center,
- a and b are the front and rear vehicle half-wheelbases so that $L = a+b$,
- d is the vehicle track,
- h is the distance between the roll center O' and the vehicle center of gravity G,
- I_x, I_y, I_z are the roll, pitch and yaw moments of inertia,
- $P = mg$ is the gravity force on the suspended mass m, with g denoting gravity acceleration,
- F_f and F_r are the front and rear lateral forces,
- F_{n1} and F_{n2} are the normal component of the tire/ground contact forces on the vehicle left and right sides, repectively,
- F_a is a restoring force parametrized by k_r and b_r, the roll stiffness and damping coefficients:

$$\overrightarrow{F_a} = \frac{1}{h}\left(k_r\varphi_v + b_r\dot{\varphi}_v\right)\overrightarrow{y_2} \tag{2}$$

Roll stiffness k_r and distance h are assumed to be initially calibrated (see [4]). Roll damping b_r is experimentally evaluated (via a driving procedure) and the other parameters (wheelbase, weight, etc) are directly measured.

1) Motion equations: In order to derive motion equations from the yaw projection shown in Fig. 3(a), analytical expressions of lateral forces F_f and F_r must be supplied. An accurate tire model, such as the celebrated Magic formula [20], could be considered, but it would require the knowledge of numerous parameters, hardly accessible in real-time. Therefore, a simple linear tire model has here been chosen. It can be expressed as:

$$\begin{cases} F_f &= C_f(.)\alpha_f \\ F_r &= C_r(.)\alpha_r \end{cases} \tag{3}$$

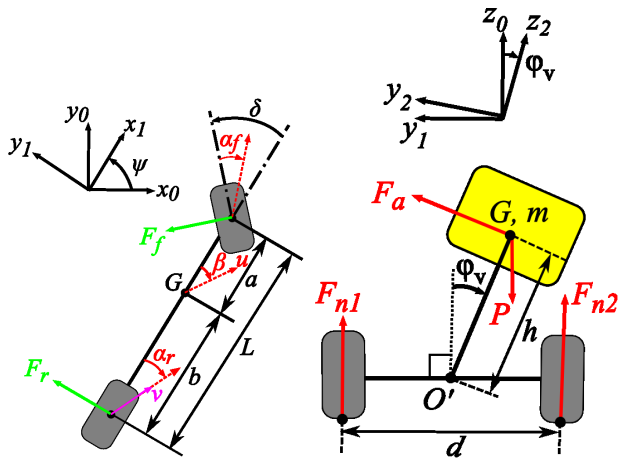

(a) Yaw projection. (b) Roll projection.

Fig. 3. Vehicle modeling.

This model requires only the knowledge of the cornering stiffnesses $C_f(.)$ and $C_r(.)$. In order to reflect both the non-linear behavior of the tire and grip condition variations, $C_f(.)$ and $C_r(.)$ are considered as slowly varying (compared to sideslip angles) and estimated in real time thanks to the mixed observer detailed in Section III. Only one parameter by wheel axle is then needed, contrary to classic tire models. As soon as cornering stiffnesses are known, the dynamic equations of the yaw model (see [31]) can be expressed as:

$$\begin{cases} \ddot{\psi} &= \frac{1}{I_z}\left(-aC_f\alpha_f\cos(\delta)+bC_r\alpha_r\right) \\ \dot{\beta} &= -\frac{1}{um}\left(C_f\alpha_f\cos(\beta-\delta)+C_r\alpha_r\cos(\beta)\right)-\dot{\psi} \\ \alpha_r &= \arctan\left(\tan(\beta)-\frac{b\dot{\psi}}{u\cos(\beta)}\right) \\ \alpha_f &= \arctan\left(\tan(\beta)+\frac{a\dot{\psi}}{u\cos(\beta)}\right)-\delta \\ u &= \frac{v\cos(\alpha_r)}{\cos(\beta)} \end{cases} \tag{4}$$

2) Rollover equations: In order to describe the rollover risk, several metrics can be computed, depending on the application, the available measurements, or the phenomenon to be described [22]. As detailed in [5], in the framework of path tracking control, robot stability can be dynamically described by the Lateral Load Transfer metric. The general expression of this metric (expressed for instance in [18] or in [1]) is given by:

$$LLT = \frac{F_{n1}-F_{n2}}{F_{n1}+F_{n2}} \tag{5}$$

where F_{n1} and F_{n2} represent the normal component of the tire/ground contact forces as shown in Fig. 3(b).

The LLT then describes the distribution of contact forces along the lateral side of the robot. It can be deduced from (5) that a unitary value of $|LLT|$ corresponds to the lift-off of the wheels on the same side of the robot. As a result, rollover risk is quite high. In the following, the robot behavior is considered as safe when the absolute value of LLT is below a threshold: $|LLT| \leq LLT_{limit}$. In order to enable the estimation and the control of such a metric, an expression of the normal forces must first be derived from the roll model (see Fig. 3(b)). With this aim several initial assumptions have been preliminary:

- The entire vehicle mass is suspended, which implies insignificant non-suspended mass (essentially tires),
- The suspended mass is assumed to be symmetrical with respect to the two planes (z_2, y_2) and (x_2, z_2). The inertial matrix is then diagonal:

$$I_{G/R_2} = \begin{bmatrix} I_x & 0 & 0 \\ 0 & I_y & 0 \\ 0 & 0 & I_z \end{bmatrix} \tag{6}$$

- Sideslip angles α_f, α_r and β are assumed to be small (corroborated by experiments),
- The vehicle velocity u at the roll center is assumed to be equal to that at the rear axle (i.e. $u \approx v$), see (4).

Using these assumptions, the *LLT* indicator can be evaluated from the Fundamental Principle of the Dynamic (FPD) applied in the $[y_2, z_2]$ plane to the overall system, subjected to four external forces (P, F_a, F_{n1} and F_{n2}). More precisely, variations of φ_v, F_{n1} and F_{n2} can be derived as:

$$\begin{aligned} \ddot{\varphi}_v &= \frac{1}{h\cos(\varphi_v)}[h\dot{\varphi}_v{}^2\sin(\varphi_v)+h\dot{\psi}^2\sin(\varphi_v)+u\dot{\psi}\cos(\beta)+ \\ &\quad \dot{u}\sin(\beta)+u\dot{\beta}\cos(\beta)-\left(\frac{k_r\varphi_v+b_r\dot{\varphi}_v}{mh}\right)\cos(\varphi_v)] \end{aligned} \tag{7}$$

$$\begin{aligned} F_{n1}+F_{n2} &= m\left[-h\ddot{\varphi}_v\sin(\varphi_v)-h\dot{\varphi}_v{}^2\cos(\varphi_v)+g\right. \\ &\quad \left.-\left(\frac{k_r\varphi_v+b_r\dot{\varphi}_v}{mh}\right)\sin(\varphi_v)\right] \end{aligned} \tag{8}$$

$$\begin{aligned} F_{n1}-F_{n2} &= \frac{2}{d}\left[I_x\ddot{\varphi}_v+(I_z-I_y)\left[\dot{\psi}^2\cos(\varphi_v)\sin(\varphi_v)\right]\right. \\ &\quad \left.-h\sin(\varphi_v)(F_{n1}+F_{n2})\right] \end{aligned} \tag{9}$$

In order to infer the roll angle and the LLT from (7)-(9), the global sideslip angle and the yaw rate are both required. Since the former cannot be measured, an observer was designed and is presented below.

III. Estimation of Grip Conditions and Indirect Measurement of Variables

As was pointed out in Section II, models may describe accurately both the robot motion and the stability metric as soon as certain variables representative of sliding effects can be known: front, rear and global sideslip angles. Unfortunately, such variables are not easily accessible to direct measurement. It has been shown, for instance in [12], that they can be estimated using only the extended model (1). Nevertheless, a mere kinematic approach for observation purposes does not encompass the entire robot dynamic and leads to a low-reactivity estimation, suitable at low speeds (up to $3m/s$), but inefficient at higher velocities because of the delay thus introduced in the control laws.

This paper is focused on off-road mobile robots moving at relatively high speed, and a more reactive approach is thus required, accounting for dynamic effects. A mixed observer, using kinematic and dynamic modeling, was developed in [13] and applied to the context of this paper. Its general principle is described in Fig. 4.

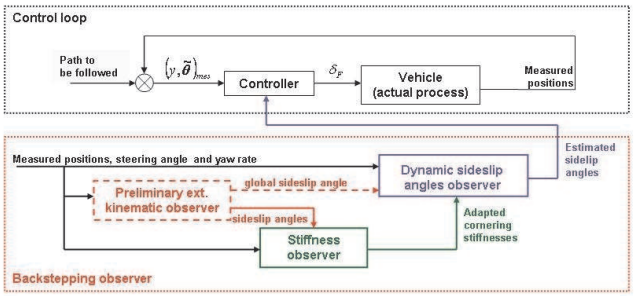

Fig. 4. Scheme of the mixed kinematic and dynamic observer

The observation loop consists of three successive steps, each one relying on the variable supplied by the previous step. Such an observation scheme enables the advantages of each modeling type to be exploited: the accuracy and reactivity of dynamic models and the simplicity (in terms of required parameters) of the kinematic representation. The calculation step are detailed in [13] and are summarized below.

A. Step 1: Preliminary sideslip angle estimation

The first step in the observation algorithm consists of estimating preliminary values for sideslip angles from the extended kinematic model (1), in order to feed the dynamic motion equations.

For path tracking to be performed, mobile robots have to be equipped with a localization device. Measurements of variables s, y and $\tilde{\psi}$ are therefore available and only the two sideslip angles α_f and α_r are unknown in the extended kinematic model (1). Since two variables have to be estimated, a 2-dimensional observation model is introduced, consisting of the second and third equations of model (1) associated with robot lateral motion. The state vector of this observation model is denoted $X_{obs} = (y, \tilde{\psi})_{obs}$, the variables v and δ are treated as measured variables and $U_{obs} = (\alpha_f, \alpha_r)$ is regarded as the control vector of the observation model. It has been shown that a non-linear control law can be designed for U_{obs} so that the observation model state vector X_{obs} exponentially converges on the actual values $X_{mes} = (y, \tilde{\psi})_{mes}$ supplied by the robot sensors. Such a control law therefore ensures that the observation model is representative of the robot's actual behavior, and consequently U_{obs} can be regarded as an estimation of the actual sideslip angles.

Nevertheless, this first sideslip angle estimation cannot be as accurate as desired since dynamic effects are neglected. For instance, mobile robot inertia, which is not accounted for in the extended kinematic model (1), introduces some delay when the robot is turning. Such an effect is falsely interpreted as sliding by this observer, generating transient irrelevant values for sideslip angles. This preliminary estimation is however satisfactory at low speed or during steady state motion.

B. Step 2: Cornering stiffness observation

When considering the dynamic model (4), the unknown variables are solely the cornering stiffnesses C_f and C_r: $\dot{\psi}$, v and δ can be measured, a preliminary estimate of the front and rear sideslip angles, denoted $\bar{\alpha}_f$ and $\bar{\alpha}_r$ in the following, was obtained in step 1, and a preliminary estimate of the global sideslip angle, denoted $\bar{\beta}$, can then be inferred from the third and fourth equations in model (4):

$$\bar{\beta} = \frac{b\bar{\alpha}_f + a\bar{\alpha}_r + b\delta}{L} \tag{10}$$

Since 2 variables have to be estimated, again a 2-dimensional observation model is considered, consisting of the first and second equations of model (4) associated with robot yaw motion. For this second observation model, the state and control vectors are respectively $X_1 = [\hat{\dot{\psi}}_1 \;\; \hat{\beta}_1]^T$ and $U_1 = [C_f \;\; C_r]^T$. v and δ are still treated as measured variables, so that the observation model equations (deduced from (4)) are:

$$\dot{X}_1 = A_1 X_1 + B_1 U_1 \tag{11}$$

where:

$$A_1 = \begin{bmatrix} 0 & 0 \\ -1 & 0 \end{bmatrix}, \quad B_1 = \begin{bmatrix} -\frac{a\bar{\alpha}_f \cos(\delta)}{I_z} & \frac{b\bar{\alpha}_r}{I_z} \\ -\frac{\bar{\alpha}_f \cos(\delta)}{um} & -\frac{\bar{\alpha}_r}{um} \end{bmatrix} \tag{12}$$

Matrix B_1 is properly defined provided that robot velocity is non-null, which is always assumed in path tracking applications.

Then, following the same approach as in step 1, a control law is designed for U_1 so that the observation model state vector X_1 exponentially converges on a vector $\bar{X}$ representative of the robot's actual behavior, namely $\bar{X} = [\tilde{\dot{\psi}} \;\; \bar{\beta}]^T$ where $\tilde{\dot{\psi}}$ is the measured yaw rate supplied by robot sensors and $\bar{\beta}$ is the global sideslip angle estimated in step 1 (see (10)). This control law ensures that observation model (11) is representative of the robot's actual behavior, so that U_1 can be regarded as an estimation of the actual cornering stiffnesses. The control law is properly defined provided that the robot is turning (since obviously cornering stiffnesses, representative of robot yaw motion, cannot be evaluated when the robot is moving in a straight line). Thus, when the robot is not turning, this second observer has to be frozen, and cornering stiffnesses are then kept equal to their previous values (this is not a serious concern, since sliding is very limited in these situations).

$\bar{\beta}$ has been used as a set point for this observer, although it may present delayed values (as explained in step 1). First, the impact of these delays may be reduced by imposing a sharper convergence on $\tilde{\dot{\psi}}$ (a reliable measurement) rather than on $\bar{\beta}$ when tuning observer gain. Secondly, the quite relevant cornering stiffness estimate obtained in this step may, in turn, be used in the last step to refine sideslip angle estimation.

C. Step 3: Sideslip angle estimation

Since cornering stiffness estimates were provided in step 2, the first two equations in model (4) can now be regarded more classically as a state space model whose state and control vectors are $X_2 = [\dot{\psi} \;\; \beta]^T$ and δ. Moreover, since sideslip angles, as well as the steering angle, never exceed quite small values, trigonometric functions can be linearized, so that robot yaw model (4) can be presented as:

$$\dot{X}_2 = A_2 X_2 + B_2 \delta \tag{13}$$

where:

$$A_2 = \begin{bmatrix} \frac{-a^2C_f - b^2C_r}{uI_z} & \frac{-aC_f + bC_r}{I_z} \\ -\frac{aC_f - bC_r}{u^2m} - 1 & -\frac{C_f + C_r}{um} \end{bmatrix}, \quad B_2 = \begin{bmatrix} \frac{aC_f}{I_z} \\ \frac{C_f}{um} \end{bmatrix} \tag{14}$$

A standard observer can then be designed to estimate the global sideslip angle. Once more, the measurement vector used to drive this estimation is $\bar{X} = [\bar{\psi} \;\; \bar{\beta}]^T$. The global sideslip angle $\bar{\beta}$ obtained in step 1 (see (10)) is still used as a virtual measurement, since its value during steady state motion is always relevant. However, in order to track sideslip angle variations accurately at transient phases, a sharper convergence on the reliable measurement $\bar{\dot{\psi}}$ is again imposed when tuning observer gain. Since dynamic effects are described in model (4), this second sideslip angle observer can display higher reactivity than the preliminary observer defined in step 1, built from the extended kinematic model (1).

More precisely, let $\hat{X}_2 = [\hat{\dot{\psi}}_2 \;\; \hat{\beta}_2]^T$ and $\tilde{X}_2 = \hat{X}_2 - \bar{X}$ denote respectively the observer state and the observer error. Then the standard observer equation associated with model (13) is:

$$\dot{\hat{X}}_2 = A_2\hat{X}_2 + B_2\,\delta + G_2\tilde{X}_2 \tag{15}$$

and combining (13) and (15) leads to the following error dynamics:

$$\dot{\tilde{X}}_2 = (A_2 + G_2)\,\tilde{X}_2 \tag{16}$$

Observer error $\tilde{X}_2$ clearly converges on zero, provided that observer gain G_2 is chosen such that $A_2 + G_2$ is negative definite. Of course, the settling time of the cornering stiffness observer defined at step 2 has to be set shorter than the settling time of this observer, so that relevant values for C_r and C_f may be available in the A_2 and B_2 matrices. In addition, G_2 has also to be tuned such that convergence on $\bar{\dot{\psi}}$ has higher priority than convergence on $\bar{\beta}$, as discussed above.

This 3-step algorithm constitutes the mixed kinematic and dynamic sideslip angle observer. In the following, $\hat{\beta}_2$ is the reactive global sideslip angle estimation to be used within the control law for robot stability, designed from roll model (7) (see Section IV-B). The front and rear sideslip angles to be used within the path tracking control law, designed from extended kinematic model (1) (see Section IV-A), can finally be obtained from the third and fourth equations in (4):

$$\begin{cases} \hat{\alpha}_r = \arctan\left(\tan(\hat{\beta}_2) - \frac{b\,\hat{\dot{\psi}}}{u\cos(\hat{\beta}_2)}\right) \\ \hat{\alpha}_f = \arctan\left(\tan(\hat{\beta}_2) + \frac{a\,\hat{\dot{\psi}}}{u\cos(\hat{\beta}_2)}\right) - \delta \end{cases} \tag{17}$$

IV. Mobile robot Control

In the proposed approach, robot control is split into two control laws, as depicted in Fig. 5. The first (upper part in the figure) is dedicated to path tracking and acts only on the front steering angle δ. The longitudinal velocity is viewed as a measured parameter, and the steering control expression is tuned with respect to the curvilinear abscissa of the robot along the reference path, so that the robot's lateral behavior is actually independent from its longitudinal velocity (as long as it is non-null). Such a property enables robot velocity to be acted upon without impacting tracking performances. Usually set to a constant value, this variable is modified in real-time if robot stability is jeopardized: robot velocity is then controlled in order to keep the LLT under a given threshold; this constitutes the second part of the approach (lower part in Fig. 5).

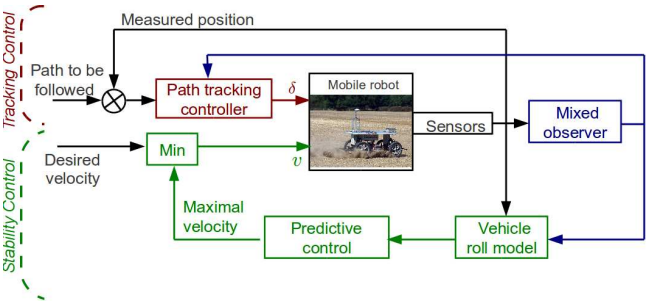

Fig. 5. Global control scheme of autonomous robot

A. Path tracking control

Since accurate sideslip angle estimates are provided by (17), all the variables in extended kinematic model (1) are therefore available. This can then be used to design a control law for the front steering angle δ so that the mobile robot converges on the desired path Γ. More precisely, the objective is to ensure the convergence of the lateral error y on zero. As detailed in [13], this objective can be accurately achieved with control law (18), designed according to the following steps:

- Since the structure of model (1) is still identical to the structure of mobile robot models derived under a non-sliding assumption, it can be converted into chained form (see [17]) via non-linear state and control transformations.
- Next, the equations describing robot lateral behavior can be converted exactly into a linear model when replacing the time derivation by a derivation with respect to curvilinear abscissa s.
- Consequently, a classical linear control approach (namely PD control) can be proposed to drive the linear system thus obtained.
- Finally, inverse state and control transformations provide the non-linear steering control expression (18).

$$\delta = \arctan\left(\tan(\hat{\alpha}_r) + \frac{L}{\cos(\hat{\alpha}_r)}\left(\frac{c(s)\cos\tilde{\psi}_2}{E} + \frac{F\cos^3\tilde{\psi}_2}{E^2}\right)\right) - \hat{\alpha}_f \tag{18}$$

with:

$$\begin{cases} \tilde{\psi}_2 = \tilde{\psi} + \hat{\alpha}_r \\ E = 1 - c(s)y \\ F = -K_p y - K_d E\tan\tilde{\psi}_2 + c(s)E\tan^2\tilde{\psi}_2 \end{cases} \tag{19}$$

Injecting steering law (18) into model (1) ensures that:

$$\frac{d^2y}{ds^2} + K_d\frac{dy}{ds} + K_p y = 0 \tag{20}$$

In view of equation (20), the exponential convergence of the mobile robot on the desired path Γ is clearly attained, and tuning control gains (K_p, K_d) enables a settling distance to be specified (since derivations within (20) are derivations with

respect to the curvilinear distance s), so that the robot's lateral behavior is actually independent from its velocity.

From a theoretical point of view, control law (18) can ensure highly accurate path tracking, whatever the shape of the desired path (since curvature $c(s)$ is explicitly taken into account within (18)), and whatever the grip conditions (since sideslip angles, reflecting current grip conditions, have been incorporated within (18)). However, in practice, the imperfections introduced by the steering actuator lead to transient overshoots at curvature transitions: for instance, when the robot enters into a curve, because of actuator delay and settling time, the steering value proposed by (18) is not instantaneously applied and the robot transiently moves away from the desired path. In order to preserve high accuracy path tracking at curvature transitions, actuator characteristics are incorporated into (18), relying on a predictive control approach. First, it can be shown (see [12]), that control law (18) can be divided into two additive terms:

$$\delta = \delta_{Traj} + \delta_{Deviation} \tag{21}$$

These terms perform two different tasks:

- δ_{Traj}: non-null term when deviations and sliding are equal to zero. This term mainly depends on reference path curvature.
- $\delta_{Deviation}$: null term when deviations and sliding are equal to zero. This term mainly depends on sliding parameters and deviations $(y, \tilde{\psi}_2)$ and ensures their convergence to 0.

As sliding conditions are unpredictable, the prediction algorithm can only be applied to δ_{Traj}. At current time t, the path curvature at time $t+H$ is inferred from the knowledge of the reference path Γ and is used to compute the objective δ^{Obj} to be attained by the actual steering angle at time $t+H$. Then, relying on Predictive Functional Control (PFC, see [24]), a control sequence for δ_{Traj} is computed with the aim of minimizing, in time window $[t, t+H]$, the quadratic difference between a desired variation for the actual steering angle attaining δ^{Obj} at $t+H$ and the steering angle variation computed over $[t, t+H]$ from the actuator model. The first term of this optimum control sequence, called δ^{Pred}_{Traj}, is then substituted for the previous trajectory term δ_{Traj}, leading to the following overall control law expression:

$$\delta \quad = \quad \delta^{Pred}_{Traj} + \delta_{Deviation} \tag{22}$$

This approach enables curvature variations to be anticipated: for instance, if the robot is supposed to enter a bend, a set point corresponding to the future curvature is sent (via the term δ^{Pred}_{Traj}) to the steering actuator some instants before the robot actually enters into the bend. The actual steering angle can then reach its expected value at the right moment, compensating for the actuator settling time and delay. Of course, the perturbations and other phenomena are still accounted by the reactive term $\delta_{Deviation}$, allowing sliding and unexpected errors to be compensated for. The overall control law (22) can then achieve high accuracy path tracking whatever the grip conditions and whatever the reference path shape, as shown in the results section.

B. Lateral Load Transfer limitation

Path tracking was addressed in Section IV-A solely as a steering control design problem. However, velocity control also has to be considered: a reference path can be tracked at limited speed by an actual robot, but not at higher speeds, since the robot wheels may then take off in the curved parts of the path and the robot may roll over, i.e. the path may no longer be achievable safely at high speed. The maximum velocity ensuring that the path may be safely followed cannot be computed *a priori* from geometrical considerations, since it clearly depends on grip conditions that are unknown and moreover varying. Consequently, in addition to the steering control law designed in the previous section, velocity control guaranteeing robot stability is now investigated.

1) Strategy of LLT limitation: In order to avoid the risk of rollover, the limitation of the LLT (i.e. $|LLT| \leq LLT_{limit}$) is considered through the control of vehicle speed. The idea is to compute at current instant t the velocity leading to LLT_{limit} at an instant $t+\bar{H}$. This value can then be considered as the maximum admissible velocity at current instant t (denoted v_{max} in the following) to avoid lateral rollover situations over the time horizon $[t, t+\bar{H}]$. Relying on this variable, the speed limitation process consists then in the following steps, shown in Fig. 5:

- The "Min" block supplies the velocity control input v_{input} to be applied to the vehicle. This variable is deduced from the comparison between the desired velocity v_d (a constant velocity is specified at the beginning of the test) and the maximum velocity v_{max}: $v_{input} = \min(v_d, v_{max})$
- The measurements shown in Fig. 5 are then used to estimate in real-time the sliding parameters and cornering stiffnesses using the mixed observer described in Section III,
- Next, these stiffnesses, the measured robot velocity and the measured steering angle are integrated into the vehicle roll model in order to compute the roll angle φ_v and the LLT (see Section IV-B2),
- Finally, the roll angle φ_v, the sliding parameters and the steering angle are processed in the "Predictive Control" block in order to supply the maximum admissible velocity v_{max} ensuring the condition $|LLT| \leq LLT_{limit}$. The computation of v_{max} is detailed in Section IV-B3. It is based on the Predictive Functional Control (PFC) formalism, detailed in [24] and applied in [32] for manipulation robotics.

2) Roll angle evolution equation : As can be seen in equations (8) and (9), the LLT does not rely explicitly on vehicle velocity, but on the roll angle; vehicle velocity is then designed to control φ_v and indirectly the LLT. As detailed in [25], the PFC formalism requires the use of linear equations. A first step then consists in linearizing the non-linear equation (7) describing the variations of φ_v. In the following, φ_{vNL} and φ_{vL} denote the roll angle supplied respectively by the non-linear model (7) and by the linear model to be derived.
In order to achieve linearization, the following assumptions are considered:

- Sideslip angles are quite small and consequently, based

on third and fourth equations in (4), the vehicle yaw rate can be approximated by:

$$\dot{\psi} = u\left(\frac{\delta+\alpha_f-\alpha_r}{L}\right) \tag{23}$$

- Since β and u are slow-varying with respect to $\dot{\psi}$, terms $u\dot{\beta}\cos(\beta)$ and $\dot{u}\sin(\beta)$ in equation (7) are largely negligible with respect to $u\dot{\psi}\cos(\beta)$ (corroborated by advanced simulations and experiments).

Linearization of (7) around $(\varphi_v, \dot{\varphi}_v) = (0,0)$ then leads to:

$$\ddot{\varphi}_{vL} = \frac{1}{h}\left[u^2\cos(\beta)\left(\frac{\delta+\alpha_f-\alpha_r}{L}\right) - \left(\frac{k_r\varphi_{vL}+b_r\dot{\varphi}_{vL}}{mh}\right)\right] \tag{24}$$

Since $u \approx v$ (see the fifth equation in (4)), the linear state-space model to be used in PFC algorithm is then:

$$\left\{\begin{array}{lcl} \dot{X} & = & AX+Bw \\ Y & = & CX \end{array}\right. \tag{25}$$

with the state-space vector $X = (\varphi_{vL}, \dot{\varphi}_{vL})^T$, the control variable $w = v^2$ and matrices:

$$A = \left[\begin{array}{cc} 0 & 1 \\ \frac{-k_r}{mh^2} & \frac{-b_r}{mh^2} \end{array}\right] \quad B = \left[\begin{array}{c} 0 \\ \cos(\beta)\left(\frac{\delta+\alpha_f-\alpha_r}{hL}\right) \end{array}\right]$$
$$C = \left[\begin{array}{cc} 1 & 0 \end{array}\right]$$

Relying on the Kalman criterion, the controllability of model (25) can be established provided that $\dot{\psi} \neq 0$. In other words, the linear roll angle φ_{vL} cannot be controlled when the vehicle is moving in straight line, which is quite natural. Then, close to neutral steering ($|\delta|$ below some steering limit), the PFC control algorithm is not activated and $v_{input} = v_d$ (this is not at all a limitation, since rollover never occurs in such situations).

3) Predictive maximum velocity computation : The PFC algorithm can now be applied to linear system (25) in order to derive the maximum velocity v_{max}. The general principle of the predictive approach is summarized in Fig. 6. Roughly, it consists in finding the control sequence which leads to the "best" future set point after a specified prediction horizon $\bar{H}$.

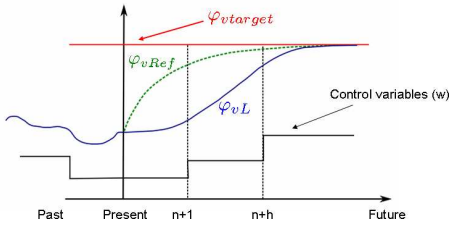

Fig. 6. Prediction principle.

More precisely, the algorithm consists of the following steps:

- The first step consists in computing the roll angle value, denoted $\varphi_{vtarget}$ in the following, leading to a LLT steady state value equal to a chosen critical threshold LLT_{limit}. Relying on the following assumptions: $\ddot{\varphi}_v = \dot{\varphi}_v = 0$ and $\xi_1 = (I_z - I_y)[\dot{\psi}^2\cos(\varphi_v)\sin(\varphi_v)]$ is largely negligible with respect to $\xi_2 = h\sin(\varphi_v)(F_{n1}+F_{n2})$ (in view of mobile robot properties and actual conditions; the magnitude of ξ_1 stays below $100\sin(\varphi_v)$, while the magnitude of ξ_2 is at least equal to $3000\sin(\varphi_v)$); it can be derived from equations (8) and (9) that:

$$|LLT| = \left|\frac{F_{n1}-F_{n2}}{F_{n1}+F_{n2}}\right| \approx \left|\frac{2}{d}h\sin(\varphi_v)\right| \tag{26}$$

As a result:

$$\varphi_{vtarget} = \pm\arcsin\left(\frac{d}{2h}LLT_{limit}\right) \tag{27}$$

- Next, a desired variation φ_{vRef}, joining the current state φ_{vNL} to $\varphi_{vtarget}$ within the prediction horizon, is defined. Typically a first order discrete system is considered:

$$\varphi_{vRef_{[n+i]}} = \varphi_{vtarget} - \gamma^i.\left(\varphi_{vtarget} - \varphi_{vNL_{[n]}}\right) \tag{28}$$

The subscripts $[n]$ and $[n+i]$ (with $0 \leq i \leq \bar{h}$) denote respectively the current time instant t and successive time instants up to $t+\bar{H}$ (since $[n+\bar{h}]$ corresponds to time instant $t+\bar{H}$) and γ is a parameter tuning the settling time for the desired variation φ_{vRef} to reach the set point $\varphi_{vtarget}$ (with $\gamma \in]0,1[$).

- Then, at current time sample $[n]$, an optimal control sequence $(w_{[n]}, \ldots, w_{[n+\bar{h}]})$ bringing φ_{vL} to $\varphi_{vtarget}$ is computed through the minimization of a quadratic criterion hereafter noted $D_{[n]}$:

$$D_{[n]} = \sum_{i=1}^{\bar{h}}\left(\widehat{\varphi_{vL}}_{[n+i]} - \varphi_{vRef_{[n+i]}}\right)^2 \tag{29}$$

where $\widehat{\varphi_{vL}}_{[n+i]}$ denotes the predicted roll angle obtained from linear model (25) and a control sequence chosen as a linear combination of some base functions:

$$w_{[n+i]} = \sum_{k=1}^{n_B}\mu_{k_{[n]}}w_{Bk_{[i]}}, \quad 0 \leq i \leq \bar{h} \tag{30}$$

where $\mu_{k_{[n]}}$ are the coefficients to be supplied by the minimization of $D_{[n]}$, n_B is the number of base functions and w_{Bk} are the base functions, generally chosen as polynomials:

$$w_{Bk_{[i]}} = i^{k-1}, \quad \forall k \tag{31}$$

Finally, since the linearization of equation (7) introduces some approximations that necessarily impair the accuracy of the predicted values of the roll angle and thus of the LLT, the criterion eventually minimized is the extended criterion $D_{2[n]}$, incorporating the current and expected discrepancies between the roll angle values supplied by the nonlinear model (7) and the linear model (25):

$$D_{2[n]} = \sum_{i=1}^{\bar{h}}\left(\widehat{\varphi_{vL}}_{[n+i]} + \widehat{e}_{[n+i]} - \varphi_{vRef_{[n+i]}}\right)^2 \tag{32}$$

where the future model error $\widehat{e}_{[n+i]}$ is defined as:

$$\widehat{e}_{[n+i]} = e_{[n]} = \varphi_{vNL_{[n]}} - \varphi_{vL_{[n]}}, \quad 1 \leq i \leq \bar{h} \tag{33}$$

If the optimal control sequence obtained from the minimization of $D_{2[n]}$ was applied over the prediction horizon, then φ_{vL} and LLT would reach respectively $\varphi_{vtarget}$ and LLT_{limit} at time sample $[n+\bar{h}]$. Therefore, the first element of the control sequence, i.e. $w_{[n]}$, has to be considered as the maximum

control input value, and the maximum vehicle velocity at current time sample $[n]$ is defined as:

$$v_{max} = \sqrt{w_{[n]}} \tag{34}$$

The PFC algorithm comprises two parameters to be tuned: the gain γ (specifying the shape of the desired variation) and the prediction horizon H.

V. Results

A. Experimental setup

The electric off-road vehicle depicted in Fig. 7 is used as an experimental platform. Designed for all-terrain mobility, it can climb slopes of up to 45°, its maximum speed is 7 $m.s^{-1}$, and it has the following properties:

Total mass	$m = 350$ kg
Yaw inertia	$I_z = 270$ kg.m^2
Wheelbase	$L = 1.2$ m
Rear half-wheelbase	$b = 0.58$ m
Maximum steering angle	$\delta_{max} = \pm 20°$
$\rightarrow$ *minimum radius of curvature*	$R_{min} = \frac{L}{\tan(\delta_{max})} = 3.3$ m

TABLE I
Experimental robot dynamic parameters

The main exteroceptive sensor on-board is a "Magellan ProFlex 500" RTK-GPS receiver, which supplies absolute position measurements accurate to within 2 *cm* at a 10 *Hz* sampling frequency. The GPS antenna is located vertically above the center of the rear axle, so that the absolute position of the point to be controlled is straightforwardly provided by the sensor. In addition, a gyrometer supplying a yaw rate measurement accurate to within $0.1°/s$ is fixed to the chassis.

Fig. 7. Experimental platform

In order to highlight the performances of the proposed control strategy, both in terms of tracking accuracy and stability, the reference path depicted in Fig. 8 was recorded manually, at a velocity of 1 $m.s^{-1}$. It is composed of two successive circles: one to the right, performed on asphalt, and the other to the left, performed on wet grass. Such a reference path was chosen since it enables several critical points to be investigated:

- The short path between the two circles is penalizing from the curvature variation point of view, thus testing the capabilities of the predictive part of the path tracking control law.
- The modification in grip conditions over the course of the path (from asphalt to grass) allows the efficiency of the sideslip angle observer and of the adaptive part of the path tracking control law to be invesstigated.
- The radius of the two circles is 5m, close to R_{min} (see Table I). Consequently, within the admissible velocity range (i.e. $v \leq 7\ m.s^{-1}$), hazardous situations from the stability point of view may be encountered (the *LLT* can reach a significant value when performing the desired circles, depending on the grip conditions). Nevertheless, the maximum steering angle δ_{max} may also be attained at high speed, so this path may then no longer be achievable.

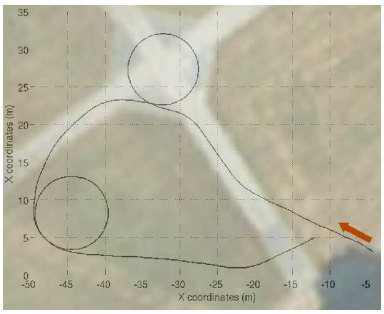

Fig. 8. Reference trajectory manually recorded

B. Results with a medium desired speed $v_d = 4m.s^{-1}$ $(14.4km.h^{-1})$

The performances of the proposed algorithms were first investigated with a medium target speed $v_d = 4m.s^{-1}$. At such a velocity, perturbations are not very significant and the chosen reference path can be completed with respect to the steering actuator limitations.

1) Motion control results: First, the velocity control for robot stability was turned off. The performance of the path tracking control law (22) is indicated in Fig. 9 by a solid red line. It can be noticed that despite the modification in grip conditions (from asphalt (up to curvilinear abscissa 90m) to grass (beyond 90m)) and the quick variations in reference path curvature, the maximum recorded error is equal to 0.5m: tracking error satisfactorily remains around zero (robot position is superposed with the reference path) within a limited area, even during fast curvature variations.

For the sake of comparison, the result obtained with a classic predictive controller neglecting sliding (which can be obtained by setting $(\hat{\alpha}_r, \hat{\alpha}_f) = (0,0)$ in control law (22)) is shown by a black dotted line in Fig. 9. Larger deviations (exceeding 1m) can be noticed, and moreover the tracking error is not centered around zero during curves. This clearly demonstrates the contribution of the grip condition and sideslip angle estimation.

The only significant errors recorded when using control law (22) are overshoots encountered at the beginning/end of

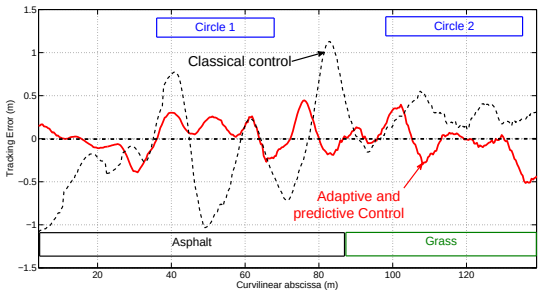

Fig. 9. Tracking error at $4m.s^{-1}$

the two circles (i.e at curvilinear abscissas $38m$, $65m$, $95m$ and $135m$). These can be explained by a slight error in the identification of the steering actuator settling time (used in the predictive part of the path tracking control law). However, they are mainly due to the settling time of the sideslip angle observer, as can be verified from the real-time cornering stiffness estimation shown in Fig. 10. It can first be seen that during both circles, cornering stiffness adaptation is satisfactory: C_f and C_r converge on $14\,000N.rad^{-1}$ when the robot moves on asphalt and beyond $16\,000N.rad^{-1}$ when it moves on grass. In contrast, adaptation is quite limited during straight line sections, since the observer is not sufficiently excited (see Section III). This is particularly true before the first curve (i.e. before curvilinear abscissa $38m$): during this part, estimated cornering stiffnesses stay around initial values, manually set to $5\,000N.rad^{-1}$ to initialize the algorithm. This arbitrary value corresponds to low grip conditions and is not representative of the actual ground contact. As soon as the robot enters the curve, the observer is excited and cornering stiffnesses converge to relevant values (from curvilinear abscissas $38m$ to $62m$). The convergence time then explains the overshoot recorded in Fig. 9 at the beginning of the first circle.

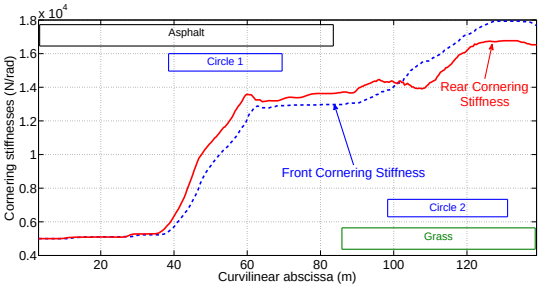

Fig. 10. Estimated cornering stiffnesses

2) Stability control results: When $v_d = 4m.s^{-1}$, the rollover risk is not high. Consequently, in order to investigate the capabilities of the LLT limitation algorithm introduced in Section IV-B, the threshold LLT_{limit} was tuned very low : $LLT_{limit} = 0.3$. The velocity applied during the third path tracking experiment was then the minimum chosen between $v_d = 4m.s^{-1}$ and v_{max}, computed according to (34). The results comparing the LLT recorded during the first path tracking experiment (with sliding estimation but without LLT limitation) and during this third experiment (with sliding estimation and LLT limitation) are shown at the top of Fig. 11 (respectively by a black plain line and a red dotted line).

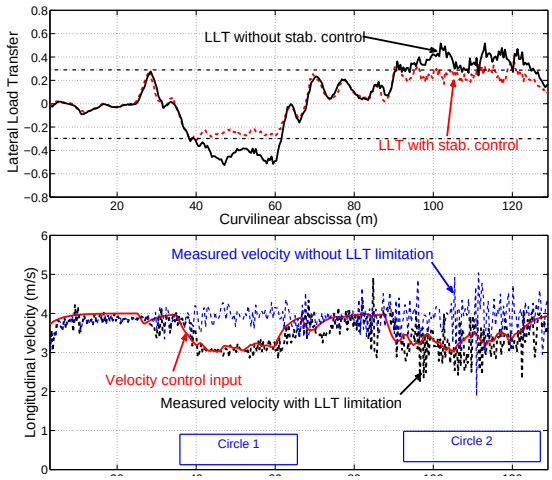

Fig. 11. Speed limitation and corresponding LLT recorded with a target velocity of $4m.s^{-1}$

It can first be noticed that, during both circles, the LLT is satisfactorily limited to the chosen value ± 0.3 when LLT limitation is active, while -0.5 and $+0.4$ are recorded during the first and the second circle respectively if LLT limitation is inactive. The robot velocities recorded during both experiments are shown at the bottom of Fig. 11: in the first experiment (without LLT limitation), robot velocity is kept around $v_d = 4m.s^{-1}$ as expected (blue dotted line). In contrast, in the third experiment, the computed v_{max} value (red solid line) is actually applied in order to limit LLT to the desired threshold ± 0.3: the robot velocity is decreased to $3m.s^{-1}$ during the first circle (on asphalt), and to a slightly higher value $3.5m.s^{-1}$ during the second one (on grass). Since the circle radii are the same, the difference in the computed maximum velocities, leading to the same LLT value, is only due to variations in grip conditions. One can also note the noise difference in the recorded signals between the two kinds of terrain.

Finally, it can be verified that the velocity control law imposing a limitation on LLT values, and therefore ensuring robot stability, does not impair path tracking accuracy: tracking error recorded when LLT limitation is inactive (plain red line) and active (black dotted line) are compared in Fig. 12.

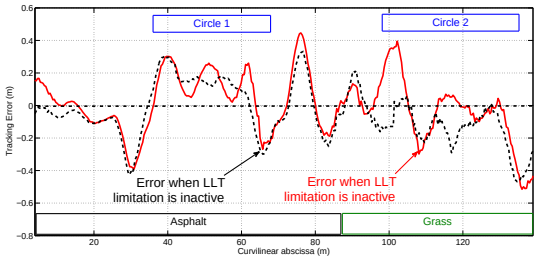

Fig. 12. Comparison of tracking errors when LLT is active/inactive

It can be seen that both errors are quite similar: the tracking

accuracy is even slightly higher and the error signal oscillates less when LLT limitation is active, since the velocity is lower, and consequently the perturbations due to shocks and steering actuator settling time are less significant.

C. Results at maximum admissible velocity

1) Motion control without LLT limitation: The satisfactory results reported in Section V-B1 were confirmed in several other experiments, with different trajectories and on different kinds of ground (see for instance [13]): tracking accuracy can actually be preserved, even at higher speed, provided that the steering actuator limitations are not reached. For the reference path shown in Fig. 8, actuator limitations are met when the robot's target velocity is $v_d = 6m.s^{-1}$: at that speed, the sliding effects are quite significant and impose large values for the steering angle, exceeding δ_{max}, so that this trajectory is no longer performable. This is illustrated in Fig. 13, where the tracking error is shown at the top of the figure, while target and measured steering angles are compared at the bottom.

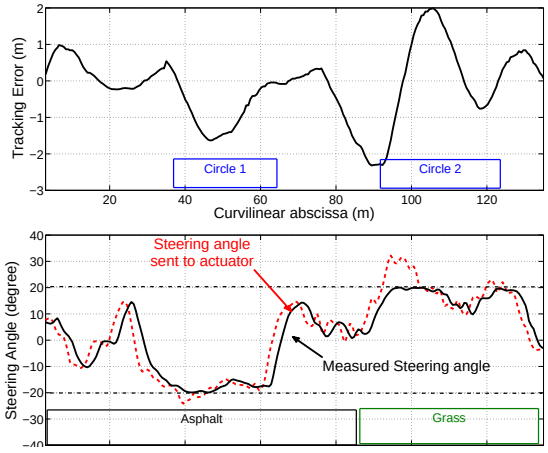

Fig. 13. Tracking error and steering angle during tracking at $6m.s^{-1}$

It can be noticed that the steering angle values sent to the actuator exceed $\pm\delta_{max}$ (i.e. $\pm 20^{\circ}$) around curvilinear abscissas $38m$ and $95m$, i.e. when the robot enters the circles. Of course, tracking accuracy is then diminished: the first steering saturation occurring at the entrance to the first circle generates an overshoot, but the tracking error then converges on zero. In contrast, at the entrance to the second circle, some oscillations are recorded, since the target steering angle values are larger. With respect to robot steering capabilities, this path with its associated grip conditions is not attainable at $6m.s^{-1}$, and therefore discussions on tracking performances would have here no meaning. Such an experiment is however quite interesting in order to investigate further the capabilities of the stability control law.

2) Stability control: The computed LLT recorded during this experiment is shown by a plain black line at the top of Fig. 14 and the corresponding measured velocity (roughly maintained around $v_d = 6m.s^{-1}$) is shown by a blue dotted line at the bottom of the same figure. It can be noticed that the critical value $LLT = 1$ is reached during the second circle, at curvilinear abscissas $100m$ and $128m$: at these instants, two wheels of one side of the robot lift off, so that the robot is very close to rollover; its stability is critical.

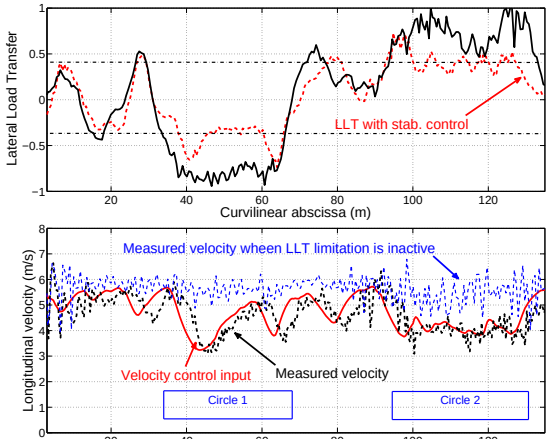

Fig. 14. Speed limitation and corresponding LLT recorded with a target velocity of $6m.s^{-1}$

In order to investigate the performances and the benefits of the proposed stability control law, the same path tracking experiment was finally carried out with LLT limitation turned on, the threshold LLT_{limit} set to 0.4, and the prediction horizon H set to $0.8s$ (i.e. equal to the steering actuator settling time). The LLT recorded during this last test is indicated by a red dotted line in Fig. 14. It can be noticed that the LLT is satisfactorily stabilized around the target values ± 0.4 during each circular part of the reference trajectory, rather than increasing to high and dangerous values when the stability control law is not used (stabilized around -0.9 during the first circle and oscillating between 0.6 and 1 during the second). Some overshoots can nevertheless be recorded when the reference path curvature varies quickly (beginning/end of circles at curvilinear abscissas $38m$, $65m$ and $95m$). These are mainly due to the settling time of the motors, as can be observed at the bottom of Fig. 14: the actual robot velocity (black dotted line) does not instantaneously reach the target velocity (solid red line), and such a delay in the actual velocity directly impacts LLT behavior. The LLT reaches -0.6 and 0.6 when the robot enters the first and the second circles respectively (curvilinear abscissas $38m$ and $95m$), before converging on the target values ± 0.4.

The general principle of the stability control law is clearly illustrated in Fig. 14. During the straight sections of the reference path (before $38m$, between curvilinear abscissas $65m$ and $95m$, and after $134m$), the robot goes almost straight, so its velocity can safely be increased up to $v_d = 6m.s^{-1}$. The velocity control input is however not constantly equal to v_d, since in order to reject sliding effects the steering angle value is not always close to zero, such that the computed value v_{max} may then be inferior to v_d. In contrast, during the circular parts of the reference path, the robot's velocity is reduced (to $5m.s^{-1}$ and $4m.s^{-1}$ in the first and second circles, respectively) so that the LLT is limited to LLT_{limit}. It can be noticed that limiting the speed to $4m.s^{-1}$ in the second circle corresponds exactly to

the conditions of the first experiment (see Section V-B1): when $v_d = 4m.s^{-1}$ and LLT limitation is inactive, the LLT reaches the value 0.4. If LLT limitation is active and $LLT_{lim} = 0.4$, the predictive control strategy then leads to $v_{max} = 4m.s^{-1}$, as expected.

VI. Conclusion

This paper proposes a path tracking approach for fast off-road mobile robots, ensuring both path tracking accuracy and robot stability. This is achieved via an algorithm acting independently on the two control variables of the robot: steering angle for motion control and robot velocity to limit rollover risk (Lateral Load Transfer limitation). Via a grip condition observer, the proposed approach accounts for sliding effects, which impact the robot's dynamics for both motion and stability control. Moreover, Predictive Functional Control is used to compensate for steering actuator delays (generating overshoots) and to anticipate rollover risk. Such a control strategy ensures high-accuracy path tracking and limits Lateral Load Transfer, whatever the shape of the trajectory and the ground conditions. These capabilities were investigated through full-scale experiments, on a trajectory covering different ground conditions and leading to hazardous situations at attainable velocities. This shows the efficiency of the proposed developments in different conditions with a limited number of sensors.

As was pointed out in the modeling section, the approach is currently limited to a flat terrain, since an estimation of actual ground inclination is not yet available. Nevertheless, theoretical work introducing a bank angle is being developed, but only tested in simulation at present, since a measurement of this variable is required. Therefore, this new work is focused on the real-time estimation of this variable by using all the axes available in an IMU (only the yaw rate is considered in the present paper).

The influence of steering actuator characteristics has also been highlighted in the present work. However, any constraint on an actuator or on robot capabilities also has an influence on tracking accuracy: for instance, settling times or inertial effects are parameters that can make a path recorded at $1m.s^{-1}$ (or computed from a map) unattainable at higher speeds. As a result, the extension of the speed limitation algorithm in order to ensure path achievability is under investigation. More precisely, the aim is to develop a second predictive algorithm to derive the maximum velocity leading to the maximum steering angle or to a robot spin situation. Such developments will ensure robot stability, not only from the rollover point of view, but also as regards dynamics.

Acknowledgment

This work is supported by French National Research Agency (ANR), grant ANR-2010-VPTT-0008-01 attributed to the ActiSurTT project. This work has been sponsored by the French government research programm Investissements d avenir through the IMobS3 Laboratory of Excellence (ANR-10-LABX-16-01), by the European Union through the programm Regional competitiveness and employment 2007-2013 (ERDF â Auvergne region), and by the Auvergne region.

References

[1] J. Ackermann and D. Odenthal. Advantages of active steering for vehicle dynamics control. In *International Conference on Advances in Vehicle Control and Safety (AVCS)*, Amiens, France, 1998.

[2] A. Astolfi, P. Bolzern, and A. Locatelli. Path-tracking of a tractor-trailer vehicle along rectilinear and circular paths: a lyapunov-based approach. *IEEE Transactions on Robotics and Automation*, 20(1):154–160, 2004.

[3] R. Bosch. *Safety, comfort and convenience systems*. Wiley, Hoboken, U.S.A., 2006.

[4] N. Bouton, R. Lenain, B. Thuilot, and J-C. Fauroux. A rollover indicator based on the prediction of the load transfer in presence of sliding: application to an all terrain vehicle. In *International Conference on Robotics and Automation (ICRA)*, pages 1158–1163, Roma, Italy, 2007.

[5] N. Bouton, R. Lenain, B. Thuilot, and P. Martinet. An active anti-rollover device based on predictive functional control : Application to an all-terrain vehicle. In *International Conference on Robotics and Automation (ICRA)*, Kobe, Japan, 2009.

[6] L. M. Corradini, T. Leo, and G. Orlando. Experimental testing of a discrete-time sliding mode controller for trajectory tracking of a wheeled mobile robot in the presence of skidding effects. *Journal of Robotic System*, 19(4):177–188, 2002.

[7] B. d'Andréa Novel, G. Campion, and G. Bastin. Control of nonholonomic wheeled mobile robots by state feedback linearization. *International Journal of Robotics Research*, 14(6):543–559, 1995.

[8] A. Diaz-Calderon and A. Kelly. *Development of a terrain adaptive stability prediction system for mass articulating mobile robots*. "Field and service robots" series. Springer Verlag, 2006.

[9] R. Eaton, H. Pota, and J. Katupitiya. Path tracking control of agricultural tractors with compensation for steering dynamics. In *International Conference on Decision and Control (CDC)*, pages 7357–7362, Shanghai, China, 2009.

[10] P. Gaspar, Z. Szabo, and J. Bokor. The design of an integrated control system in heavy vehicles based on an LPV method. In *International Conference on Decision and Control (CDC)*, pages 6722–6727, Sevilla, Spain, 2005.

[11] R. Lenain. *Contribution à la modélisation et à la commande de robots mobiles en présence de glissement*. PhD thesis, Université Blaise Pascal, Clermont-Ferrand, France, 2005.

[12] R. Lenain, B. Thuilot, C. Cariou, and P. Martinet. Adaptive and predictive path tracking control for off-road mobile robots. *European Journal of Control*, 13(4):419–439, 2007.

[13] R. Lenain, B. Thuilot, C. Cariou, and P. Martinet. Multi-model based sideslip angle observer : Accurate control of high-speed mobile robots in off-road conditions. In *International Conference on Intelligent RObots and Systems (IROS)*, Saint-Louis, U.S.A., 2009.

[14] C.B. Low and D. Wang. Maneuverability and path following control of wheeled mobile robot in the presence of wheel skidding and slipping. *Journal of Field Robotics*, 27(2):127–144, 2010.

[15] E. Lucet, C. Grand, D. Salle, and P. Bidaud. Stabilization algorithm for a high speed car-like robot achieving steering maneuver. In *International Conference on Robotics and Automation (ICRA)*, pages 2540–2545, Pasadena, U.S.A., 2008.

[16] E. Maalouf, M. Saad, and H. Saliah. A higher level path tracking controller for a four-wheel differentially steered mobile robot. *Robotics and Autonomous Systems*, 54(1):23–33, 2006.

[17] A. Micaelli and C. Samson. Trajectory tracking for unicycle-type and two-steering-wheels mobile robots. INRIA. Technical report, n°2097, 1993.

[18] A.J.P. Miège and D. Cebon. Design and implementation of an active roll control system for heavy vehicles. In *International Symposium on Advanced VEhicle Control (AVEC)*, Hiroshima, Japan, 2002.

[19] National Highway Traffic Safety Administration (NHTSA). Trends in static stability factor of passengers cars, light trucks and vans. Technical report, U.S. Department of transportation, 2005.

[20] H. B. Pacejka. *Tire and vehicle dynamics*. Society of Automotive Engineers, 2002.

[21] E.G. Papadopoulos and D.A. Rey. A new measure of tipover stability margin for mobile manipulators. In *International Conference on Robotics and Automation (ICRA)*, pages 3111–3116, Minneapolis, U.S.A., 1996.

[22] S.C. Peters. Stability measurement of high-speed vehicles. *Vehicle System Dynamics*, 47(6):701–720, 2009.

[23] S.C. Peters and K. Iagnemma. Mobile robot path tracking of aggressive maneuvers on sloped terrain. In *International Conference on Intelligent RObots and Systems (IROS)*, pages 242–247, Nice, France, 2008.

[24] J. Richalet. Industrial applications of model based predictive control. *Automatica*, 29(5):1251–1274, 1993.

[25] J. Richalet, E. Abu, C. Arber, H. Kuntze, A. Jacubasch, and W. Schill. Predictive functional control - application to fast and accurate robots. In *IFAC World Congress*, Munich, Germany, 1997.

[26] P. Sardain and G. Bessonet. Forces acting on a biped robot. center of pressure - zero moment point. *IEEE Transactions on Systems, Man, and Cybernetics*, 34(5):630–637, 2004.

[27] H. Schafer, M. Proetzsch, and K. Berns. Action/perception-oriented robot software design: an application in off-road terrain. In *International Conference on Control, Automation, Robotics and Vision (ICARCV)*, pages 223–228, Hanoi, Vietnam, 2008.

[28] B. Schofield, T. Hagglund, and A. Rantzer. Vehicle dynamics control and controller allocation for rollover prevention. In *International Conference on Control Applications*, Munich, Germany, 2006.

[29] R. Siegwart and I.R. Nourbakhsh. *Introduction to autonomous mobile robots*. MIT Press, 2004.

[30] R. Solea and U. Numes. Trajectory planning and sliding-mode control based trajectory-tracking for cybercars. *Integrated Computer-Aided Engineering*, 14(1):33–47, 2007.

[31] J. Stéphant. *Contribution à l'étude et à la validation expérimentale d'observateurs appliqués à la dynamique du véhicule*. PhD thesis, Université de Technologie de Compiègne (UTC), France, 2004.

[32] A. Vivas and V. Mosquera. Predictive functional control of a PUMA robot. In *International Conference on Automatic Control and Systems Engineering (ACSE)*, pages 35–40, Cairo, Egypt, 2005.